Electronic Supplementary Material (ESI) for Journal of Materials Chemistry A.

SUPPORTING INFORMATION FOR

Synthesis of TiO_2 Nanotube Arrays on 3D-Printed Structures for Application in Fischer-Tropsch Synthesis Catalysts

Luis C. Caballero,[a] Joseph Brindle,[a] Nathan P. Ramey,[a] Sayed Abu Sufyan,[a] Swomitra K. Mohanty[a,b] and Michael M. Nigra[a,*]

[a]Department of Chemical Engineering, University of Utah, Salt Lake City, UT, U.S.A.

E-mail: michael.nigra@utah.edu

[b]Department of Materials Science and Engineering, University of Utah, Salt Lake City, UT, U.S.A.

Table of Contents

1. Fischer-Tropsch Reactor and Reaction Conditions

Fischer-Tropsch synthesis (FTS) using the bimetallic FeCo catalysts supported on TiO_2 nanotubes was carried out in a reactor system designed and built specifically for this work, as shown in Scheme S1 and Figure S1. The stainless-steel reactor used in this setup was cylindrically shaped and had a diameter of 9.40 mm. This tubular component was chosen due to the reduced transport distances, and it was repeatedly tested to ensure a safe operation under reaction conditions. Due to the highly exothermic nature of FTS, the reactor setup was tested to prevent potential overheating. It was also pressure-tested with N_2 for leaks in the system and all fittings. Safe operation was established, and leaks of hazardous gases involved in the process, such as CO, were prevented.

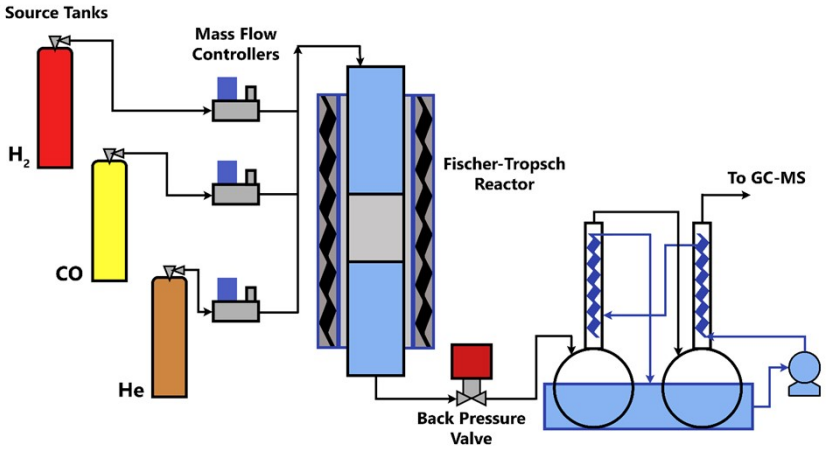

Scheme S1. FTS reactor setup diagram used to test the bimetallic FeCo catalysts supported on TiO_2 nanotubes.

The reactor system was designed to comply with the American Society of Mechanical Engineers (ASME) guidelines for vessel design, considering a maximum temperature of up to 500 °C and a maximum pressure of 30 bar (gauge). The reaction products were analyzed with an in-situ gas chromatography-mass spectroscopy (GC-MS) setup. The design consisted of the effluent stream flowing into a heated and insulated 0.25 in. line into the back pressure valve, as specified in Scheme S1. A system was written, tested, and modified, operated by Opto 22 (California, USA), to control operating conditions in the system properly. Regulators were also installed to achieve a delivery pressure of 35 atm. For the experimental runs considered in this work, the reactor was operated at a setpoint temperature of 250 °C and a pressure of 300 psi(g). The reactant mixture fed into the system consisted of an H_2:CO:He ratio of 2:1:4. The Fischer-Tropsch reactor system is shown in Figure S1.

Figure S1. FTS reactor system used in this work, with the tubular 9.40 mm stainless steel reactor.

2. CAD Modeling of Cylindrical Structures

For the FTS catalyst design, a crisscross hole pattern was chosen with the guidance of additive manufacturing experts at Stratasys Direct Manufacturing (California, USA). This design was chosen to ensure self-supporting capabilities for direct metal laser melting (DMLM). The metal 3D printer used in this work (Electro-Optical Systems (EOS) M280) was considered when modeling the structures, as it had to follow their proprietary metal additive manufacturing protocol. The final CAD model with dimensions is shown in Figure S2.

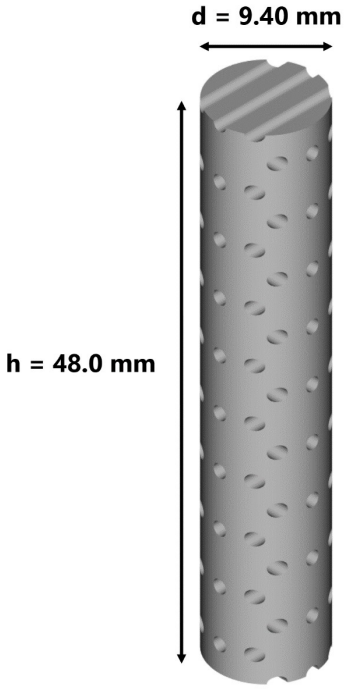

Figure S2. CAD model of cylindrical structures 3D-printed using Ti6Al4V—diameter of 9.40 mm and height of 48.0 mm.

3. Electrochemical Anodization of the Ti6Al4V Substrates: Current and Voltage Measurements

The development of the two-step anodization (TSAN) process used to synthesize TiO_2 nanotube arrays (TNAs) on the 3D-printed titanium structures required the assessment of two main variables: voltage and electric current. The method developed in this work is loosely based on the works by Ahmad et al.[1] and Lim et al.[2], in which the effect of different anodization parameters on the growth mechanism of TiO_2 nanotubes is assessed. Introducing the novel substrates 3D-printed with Ti6Al4V led to several preliminary experimental runs to assess how the aluminum and vanadium content in the alloy would affect the formation of the TNAs. The voltage and electric current were then measured and recorded at intervals to ensure consistency between the samples. Table S1 shows the measured values for these parameters for samples A, B, and C for both electrochemical runs.

Table S1. Two-step electrochemical anodization process parameters—electric current and voltage, as a function of time for Specimens A, B, and C.

First Electrochemical Run (45 min)						
Time (min)	**Specimen A**		**Specimen B**		**Specimen C**	
	Potential (V)	**Current (A)**	**Potential (V)**	**Current (A)**	**Potential (V)**	**Current (A)**
0 (initial)	60.02	0.010	60.02	0.008	60.02	0.009
5	60.03	0.005	60.03	0.003	60.02	0.007
10	60.03	0.006	60.06	0.007	60.02	0.006
15	60.04	0.007	60.04	0.009	60.03	0.009
20	60.05	0.008	60.03	0.012	60.04	0.009
25	60.05	0.009	60.03	0.010	60.05	0.010
30	60.05	0.009	60.03	0.009	60.03	0.009
35	60.05	0.010	60.03	0.009	60.03	0.010
40	60.05	0.010	60.03	0.010	60.04	0.010
45 (final)	60.05	0.011	60.03	0.011	60.04	0.011
Second Electrochemical Run (60 min)						
Time (min)	**Specimen A**		**Specimen B**		**Specimen C**	
	Potential (V)	**Current (A)**	**Potential (V)**	**Current (A)**	**Potential (V)**	**Current (A)**
0 (initial)	30.01	0.032	30.01	0.058	30.02	0.040
5	30.02	0.017	30.01	0.016	30.03	0.018
10	30.02	0.014	30.02	0.013	30.03	0.018
15	30.02	0.013	30.03	0.013	30.03	0.014
20	30.02	0.013	30.01	0.012	30.02	0.013
25	30.03	0.013	30.01	0.012	30.02	0.012
30	30.03	0.013	30.01	0.012	30.03	0.011
35	30.02	0.013	30.01	0.011	30.01	0.011
40	30.02	0.013	30.01	0.011	30.02	0.012
45	30.02	0.013	30.01	0.011	30.03	0.012
50	30.02	0.014	30.01	0.011	30.03	0.012
55	30.02	0.014	30.01	0.011	30.03	0.012
60 (final)	30.02	0.014	30.01	0.011	30.03	0.012

4. Calculation of the Average Olefin-to-Paraffin Ratio (O/P)

The olefin-to-paraffin ratio (O/R) for the Fischer-Tropsch FeCo catalysts supported on TiO_2 nanotubes (Specimen B) was calculated by running a Python code that was written and tested to streamline the analysis of the experimental gas chromatography-mass spectrometry (GC-MS) data. The O/P ratio value was recorded at specific time intervals as the reaction progressed and subsequently tabulated, as shown in Table S2. The O/P values were averaged for each data point using the individual values for all three experimental runs, and the standard deviation was calculated accordingly. The average O/P was calculated to be 0.424, with a standard deviation of ±0.078.

Table S2. Experimental data for the olefin-to-paraffin ratio (O/P) for the FeCo catalysts on TNAs (Specimen B).

Time (h)	Olefin-to-Paraffin Ratio (O/P)			
	Experimental Run #1	Experimental Run #2	Experimental Run #3	Average Value
0.15	0.5052	0.3046	0.3768	0.3955
0.20	0.5181	0.3855	0.3012	0.4016
0.40	0.5639	0.4217	0.2916	0.4257
0.60	0.6120	0.4578	0.2819	0.4506
0.80	0.6651	0.5084	0.2699	0.4811
1.00	0.7325	0.5783	0.2482	0.5197
1.20	0.7904	0.6458	0.2289	0.5550
1.40	0.7928	0.6964	0.2313	0.5735
1.60	0.6964	0.7301	0.2627	0.5631
1.80	0.5976	0.7663	0.2964	0.5534
2.00	0.5277	0.6699	0.3446	0.5141
2.20	0.4819	0.5012	0.4024	0.4618
2.40	0.4337	0.3108	0.4627	0.4024
2.60	0.3904	0.2602	0.4602	0.3703
2.80	0.3422	0.2072	0.4458	0.3317
3.00	0.3012	0.1590	0.4265	0.2956
3.20	0.2651	0.3976	0.5422	0.4016
3.40	0.2337	0.6578	0.6458	0.5124
3.60	0.2024	0.8675	0.7422	0.6040
3.80	0.1880	0.6916	0.6892	0.5229
4.00	0.1687	0.5205	0.6313	0.4402
4.20	0.1663	0.3831	0.5904	0.3799
4.40	0.2169	0.3229	0.5373	0.3590
4.60	0.2554	0.2602	0.4867	0.3341
4.80	0.2578	0.2337	0.4916	0.3277
5.00	0.2024	0.2506	0.5614	0.3382
5.20	0.1518	0.2675	0.6386	0.3526
5.40	0.1711	0.2482	0.6506	0.3566
5.60	0.2530	0.2096	0.6410	0.3679
5.80	0.3157	0.1783	0.6386	0.3775
6.00	0.3205	0.2506	0.5494	0.3735
6.20	0.3060	0.3687	0.4337	0.3695
6.40	0.2843	0.4819	0.3325	0.3663
6.60	0.3566	0.3663	0.4819	0.4016
6.80	0.4386	0.2313	0.6241	0.4313
7.00	0.5108	0.1060	0.7325	0.4498
7.20	0.5253	0.0723	0.6578	0.4185
7.40	0.5446	0.0337	0.5952	0.3912

7.50	0.5530	0.5609	0.0165	0.3768

5. Kinetic Modeling of the Fischer-Tropsch Process

The average chain growth parameter (α) for the Fischer-Tropsch FeCo catalysts supported on TiO_2 nanotubes (Specimen B) was calculated using a highly-detailed kinetic model based on heat transfer considerations due to the highly exothermic nature of the FTS reaction. Computational fluid dynamics (CDF) modeling was followed by kinetic modeling to ensure the feasibility of the process. The process parameters and kinetic variables were then considered, and an extensive literature review was conducted to select an appropriate base model for this work. The model introduced by Todic *et al.*[3] for a Re-promoted Co-based FTS catalyst was then selected. This work was deemed appropriate due to the wide availability of process parameters needed for rebuilding it and the relatively high quality of model predictions against experimental values, with a mean absolute relative residual (MARR) value of 23.5 %. The original model was developed based on the Langmuir-Hinshelwood-Hougen-Watson approach and was based on the CO-insertion mechanism for the Fischer-Tropsch process. The elementary steps for this mechanism are shown in Table S3, as adapted from their study. .

Table S3. Elementary steps in the CO-insertion mechanism for the FTS reaction.

Step Number	Elementary Step	Rate and Equilibrium Constants
(1)	$CO + S \rightleftharpoons CO\text{-}S$	K_1
(2)	$H_2 + 2S \rightleftharpoons 2H\text{-}S$	K_2
(3^{RDS})	$CO\text{-}S + H\text{-}S \rightarrow CHO\text{-}S + S$ $CO\text{-}S + CH_3\text{-}S \rightarrow CH_3CO\text{-}S + S$ $CO\text{-}S + C_nH_{2n+1}\text{-}S \rightarrow CH_3CO\text{-}S + S$, n = 2, 3…	K_3
(4)	$CHO\text{-}S + H\text{-}S \rightleftharpoons CH_2O\text{-}S + S$ $CH_3CO\text{-}S + H\text{-}S \rightleftharpoons CH_3CHO\text{-}S + S$ $C_nH_{2n+1}CO\text{-}S + H\text{-}S \rightleftharpoons C_nH_{2n+1}CHO\text{-}S + S$, n = 2, 3…	K_4
(5)	$CH_2O\text{-}S + 2H\text{-}S \rightleftharpoons CH_3\text{-}S + OH\text{-}S + S$ $CH_3CHO\text{-}S + 2H\text{-}S \rightleftharpoons CH_3\text{-}S + OH\text{-}S + S$ $C_nH_{2n+1}CHO\text{-}S + 2H\text{-}S \rightleftharpoons C_nH_{2n+1}CH_2\text{-}S + OH\text{-}S + S$, n = 2, 3…	K_5
(6)	$OH\text{-}S + H\text{-}S \rightleftharpoons H_2O + 2S$	K_6
(7^{RDS})	$CH_3\text{-}S + H\text{-}S \rightarrow CH_4 + 2S$ $C_nH_{2n+1}\text{-}S + H\text{-}S \rightarrow C_nH_{2n+2} + 2S$, n = 2, 3…	K_{7M} K_7
(8^{RDS})	$C_2H_5\text{-}S \rightarrow C_2H_4 + H\text{-}S$ $C_nH_{2n+1}\text{-}S \rightarrow C_nH_{2n} + H\text{-}S$, n = 3, 4…	K_{8E} $K_{8,n}$

RDS: rate-determining step, **S:** catalytic active site

This kinetic model was then re-built by using the procedure, equations, and process parameters stated in the literature, with the calculated values being compared to those shown in the original model. The conditions were then considered at a temperature of 229.85 °C, pressure of 1.5 MPa, H_2/CO ratio at 2.1, and a weight hourly space velocity (WHSV) of 11.3 NL/g_{cat}/h. The experimental outcomes were deemed positive and apt to be used as the starting point for the model, which was subsequently tested extensively. Experimental data for all three runs was obtained after running the Python code based on the model. A generalization was made to simplify the calculation of the α parameter for these catalysts. The Ander-Schultz Flory (ASF) distribution was used in this work to obtain the α values as a function of time. Despite negative deviations from ASF being observed for FTS in the literature[4], it is regarded as a well-accepted model, as most product distributions adhere to it[5, 6]. In this work, the α values were calculated through the generation of a least squares regression model. This parameter is described by Equation (S1), where (W) is the weight fraction of the hydrocarbons and (n) indicates the number of carbon atoms[7]:

$$\frac{W}{n} = (1-\alpha)^n(\alpha)^{1-n} \qquad \textbf{(S1)}$$

The α values of the three experimental runs for Specimen B were averaged for each time at which the data was collected, and the standard deviation was calculated as a function of these average values. Table S4 shows the

experimental data after running the catalysts. The average α value was calculated to be 0.273, with a standard deviation of ±0.143.

Table S4. Experimental data for the chain growth parameter (α) for the FeCo catalysts supported on TiO_2 nanotubes (Specimen B).

Time (h)	Chain Growth Parameter (α)			
	Experimental Run #1	Experimental Run #2	Experimental Run #3	Average Value
0.16	0.762	0.794	0.420	0.659
1.30	0.309	0.764	0.166	0.413
1.89	0.149	0.798	0.315	0.420
2.44	0.112	0.483	0.162	0.253
3.02	0.086	0.345	0.125	0.185
3.59	0.113	0.469	0.281	0.288
4.15	0.061	0.727	0.167	0.319
4.72	0.093	0.240	0.194	0.175
5.28	0.069	0.208	0.127	0.135
5.83	0.125	0.222	0.208	0.185
6.42	0.111	0.156	0.204	0.157
7.00	0.190	0.240	0.138	0.189
7.55	0.093	0.314	0.111	0.173

6. Elemental Analysis of the FeCo Fischer-Tropsch Catalysts

The elemental analysis of the FeCo catalysts was an important step in the subsequent normalization of the CO consumption rates for each experimental run. The catalysts were subjected to non-destructive X-ray fluorescence (XRF) characterization. Each sample was analyzed at two identical points on their surface using the Eagle III Microspot XRF in the Electron Microscopy and Surface Analysis Laboratory at the University of Utah, with the guidance of characterization experts. This method was selected for these applications, as the spectrometer provides sub-1.0 at. % bulk compositional analysis of large samples. Improved sensitivity was also achieved with the use of a Silicon Lithium Si(Li) detector. The data for all three experimental runs for Specimen B is shown in Table S5.

Table S5. Experimental data for the weight percent (wt. %) by mass and atomic mass for the FeCo catalysts supported on TiO_2 nanotubes (Specimen B).

Weight Percent (wt. %) by Mass							
Experimental Run	**Fe wt. %**		**Co wt. %**		**Average Fe wt. %**	**Average Co wt. %**	**Average Total FeCo wt. %**
	Spot #1	Spot #2	Spot #1	Spot #2			
#1	1.73	1.68	1.32	1.31	1.705	1.315	3.020
#2	0.12	0.09	0	0	0.105	0.000	0.110
#3	0.18	0.20	0.13	0.14	0.190	0.135	0.330
Weight Percent (wt. %) by Atomic Mass							
Experimental Run	**Fe wt. %**		**Co wt. %**		**Average Fe wt. %**	**Average Co wt. %**	**Average Total FeCo wt. %**
	Spot #1	Spot #2	Spot #1	Spot #2			
#1	1.41	1.09	1.02	0.81	1.250	0.910	2.170
#2	0.10	0.08	0	0	0.090	0.000	0.090
#3	0.14	0.16	0.10	0.11	0.150	0.100	0.260

7. Calculation of the Normalized Average Rate of CO Consumption ($-r_{CO,\ nor}$)

The experimental XRF data obtained for the elemental composition of the FeCo catalysts was used to normalize the CO consumption rates obtained from running the FTS reaction. The CO conversions for Specimen B were 66.60%, 0.84%, and 5.54% for each of the experimental runs, respectively. Due to the discrepancy between these values, the XRF data was helpful in elucidating the kinetics of the reaction as a function of active metal loading in each sample. The CO flow rate was constant for all three runs, at 25 SCCM. Using the conversion factor, 1 SCCM = 7.45 x 10^{-7} mol/s, the mole flow rate was calculated at 1.863 x 10^{-5} mol/s. The normalized average rate of CO consumption ($-r_{CO,\ nor.}$) was calculated according to Equation (S2), where $\dot{n}_{CO}$ is the molar flow rate of CO, X_{CO} is the conversion of CO, and m_{FeCo} is the mass of FeCo active phase according to the XRF data.

$$-\bar{r}_{CO,\ nor.} = \frac{\dot{n}_{CO} * X_{CO}}{m_{FeCo}} \qquad \textbf{(S2)}$$

Table S6 shows the values used to calculate $-r_{CO,\ nor.}$ for each experimental run, with units of $mol_{CO}/s{\cdot}g_{FeCo}$. The standard deviation for the normalized average rate of CO consumption for all three runs was calculated at 8.99 x 10^{-6} $mol_{CO}/s{\cdot}g_{FeCo}$.

Table S6. Experimental data for the normalized average rate of CO consumption ($-r_{CO,\ nor}$) over 8 hours time-on-stream for the FeCo catalysts supported on TiO_2 nanotubes (Specimen B).

Normalized Average Rate of CO Consumption ($-r_{CO,\ nor.}$)						
Experimental Run	**Total Mass (g)**	**Average Total FeCo wt. %**	**Mass of FeCo (g)**	**X_{CO}**	**$\dot{n}_{CO}$ (mol/s)**	**$-r_{CO,\ nor}$ ($mol_{CO}/s{\cdot}g_{FeCo}$)**
#1	11.97	3.02	0.361	0.6660	1.24 x 10^{-5}	3.43 x 10^{-5}
#2	11.91	0.11	0.013	0.0084	1.56 x 10^{-7}	1.25 x 10^{-5}
#3	12.18	0.33	0.040	0.0553	1.03 x 10^{-6}	2.60 x 10^{-5}
						2.43 x 10^{-5}

8. Average Carbon Product Distribution for Fischer-Tropsch Synthesis and Catalyst Stability

The product distribution by carbon number and hydrocarbon type (olefins and paraffins) was obtained by analyzing the GC-MS data using the Python code developed in this work. For Specimen B, the results for experimental runs 1, 2, and 3 were averaged for each carbon number and the product distribution was obtained. The data reveals the formation of both olefins and paraffins, with C_4-C_6 products not being extensively produced in the reaction. The results are shown in Figure S3.

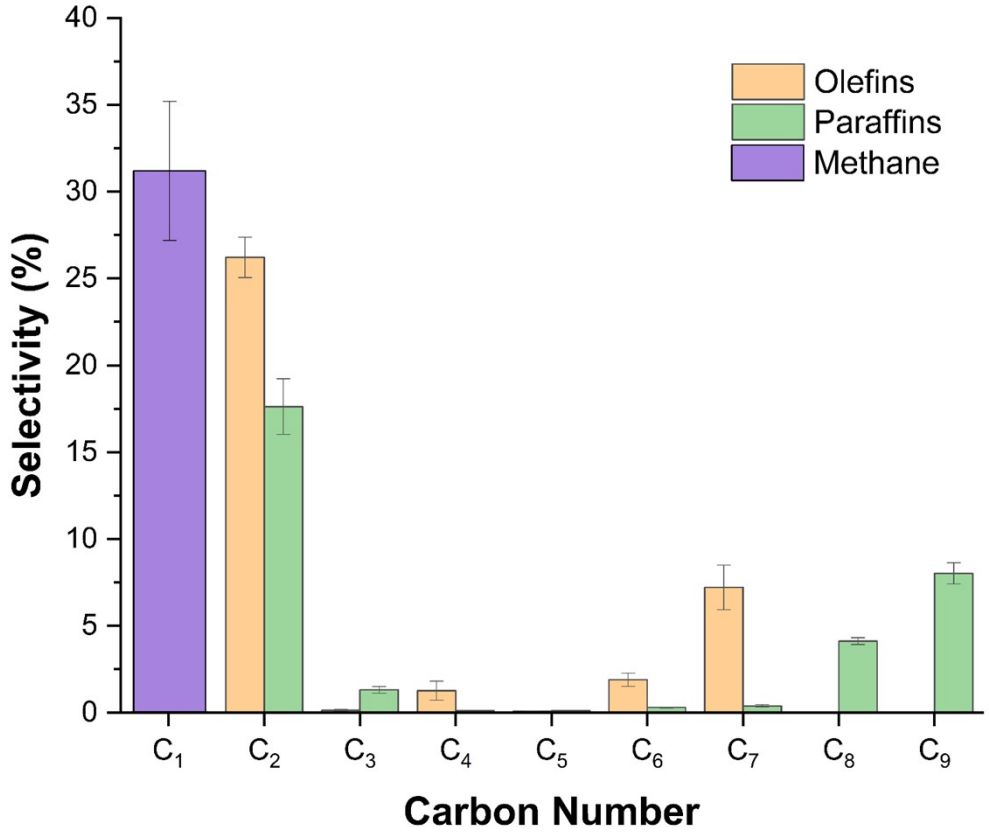

Figure S3. Experimental FTS product distribution (olefins, paraffins, and methane) for the FeCo catalysts supported on TiO_2 nanotube arrays grown on the 3D-printed titanium substrates (Specimen B).

The stability of the catalysts in this work was assessed by plotting the average normalized rate of CO consumption ($mol_{CO}/s{\cdot}g_{FeCo}$) for every data point against its time-on-stream (TOS). The results are shown in Figure S4.

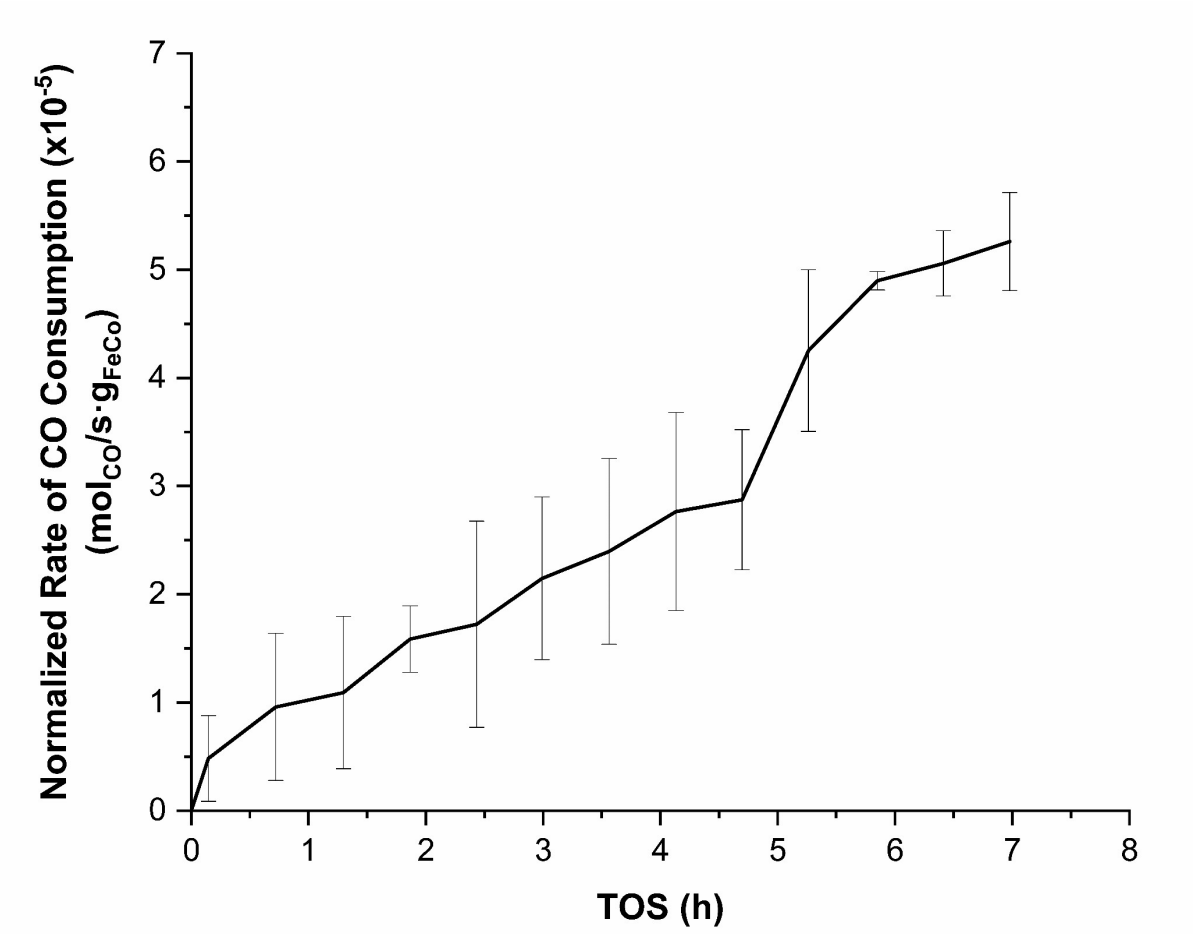

Figure S4. Average normalized rate of CO consumption ($mol_{CO}/s \cdot g_{FeCo}$) as a function of time-on-stream (TOS) (h).

References

1. A. Ahmad, E. U. Haq, W. Akhtar, M. Arshad and Z. Ahmad, *Applied Nanoscience*, 2017, **7**, 701-710.
2. Y.-C. Lim, Z. Zainal, W.-T. Tan and M. Z. Hussein, *International Journal of Photoenergy*, 2012, **2012**, 638017.
3. B. Todic, W. Ma, G. Jacobs, B. H. Davis and D. B. Bukur, *Catalysis Today*, 2014, **228**, 32-39.
4. R. Snel, *Catalysis Letters*, 1988, **1**, 327-330.
5. J. S. Albuquerque, F. O. Costa and B. V. S. Barbosa, *Catalysis Letters*, 2019, **149**, 831-839.
6. I. Puskas and R. S. Hurlbut, *Catalysis Today*, 2003, **84**, 99-109.
7. K. Cheng, J. Kang, D. L. King, V. Subramanian, C. Zhou, Q. Zhang and Y. Wang, in *Advances in Catalysis*, ed. C. Song, Academic Press, 2017, vol. 60, ch. 3, pp. 125-208.